09

Investigation of the characteristics of the InGaAs/InAlGaAs superlattice for 1300 nm range vertical-cavity surface-emitting lasers

© S.A. Blokhin,[1] A.V. Babichev,[2] A.G. Gladyshev,[2] L.Ya. Karachinsky,[1,2,3] I.I. Novikov,[1,2,3] A.A. Blokhin,[1] M.A. Bobrov,[1] N.A. Maleev,[1] A.G. Kuzmenkov,[4] A.M. Nadtochiy,[5] V.N. Nevedomskiy,[6] V.V. Andryushkin,[2] S.S. Rochas,[2] D.V. Denisov,[7] K.O. Voropaev,[8] I.O. Zhumaeva,[8] V.M. Ustinov,[4] A.Yu. Egorov,[3] V.E. Bougrov[2]

[1] Ioffe Institute,
194021 St. Petersburg, Russia
[2] ITMO University,
197101 St. Petersburg, Russia
[3] Connector Optics LLC,
194292 St. Petersburg, Russia
[4] Submicron Heterostructures for Microelectronics, Research and Engineering Center, Russian Academy of Sciences,
194021 St. Petersburg, Russia
[5] National Research University Higher School of Economics,
190121 St. Petersburg, Russia
[6] Ioffe Institute, Common use center Materials Science and Diagnostics in Advanced Technologies,
194021 St. Petersburg, Russia
[7] St. Petersburg State Electrotechnical University „LETI“
197022 St. Petersburg, Russia
[8] OAO OKB-Planeta,
173004 Veliky Novgorod, Russia
e-mail: blokh@mail.ioffe.ru

Received August 19, 2021
Revised September 2, 2021
Accepted September 3, 2021

X-ray structural analysis and photoluminescence spectroscopy techniques were used to study heterostructures based on InGaAs/InAlGaAs superlattice for active regions of 1300 nm range lasers grown by molecular beam epitaxy. It is shown that the grown heterostructures have a high crystal quality. The perpendicular lattice mismatch of the average crystal lattice constant of the InGaAs/InAlGaAs superlattice with respect to the crystal lattice constant of the InP substrate is estimated at $\sim +0.01\%$. An analysis of the photoluminescence spectra made it possible to conclude that the contribution of Auger recombination is insignificant in the studied range of excitation power density. Studies of vertical-cavity surface-emitting lasers with an active region based on the InGaAs/InAlGaAs superlattice made it possible to estimate the gain coefficient at a level of $650\,cm^{-1}$ for the standard logarithmic approximation of the dependence of the gain on the current density. The transparency current density of the laser was $400-630\,A/cm^2$, which is comparable to the record low values for the case of highly strained InGaAs–GaAs and InGaAsN–GaAs quantum wells in the spectral ranges of 1300 nm, respectively.

Keywords: superlattice, vertical-cavity surface-emitting laser, optical gain.

DOI: 10.21883/TP.2022.15.55271.240-21

Introduction

Vertical-cavity surface-emitting lasers (VCSELs) operating in the 1300 nm spectral range are promising for creating active optical cables (optical interconnects) that are needed for data transmission over relatively long distances (in excess of 1 km). Lasers of this type are also of interest in the context of hybrid integration with silicon photonics [1], fabrication of silicon photonic [2] and electronic microchips and modulators. The production of sensor systems and emission sources for optical wireless data transmission is a separate field of application of VCSELs operating in the 1300 nm spectral range [3].

Although 1300 nm range VCSELs have several important practical applications, their usability is limited by fundamental limitations set by the specifics of InAlGaAsP/InP and InAlGaAs/GaAs material systems [4]. The problems with monolithic (grown in a single epitaxial process) VCSELs on InP substrates stem from the low contrast of refraction indices and the poor thermal conductivity of layers of distributed Bragg reflectors (DBRs) in the InAlGaAsP/InP material system and from the complexity of implementation of effective current optical confinement. The problem of monolithic VCSELs on GaAs substrates stem, in turn, is the lack of active regions emitting efficiently in the wavelength range of 1250–1300 nm, although partially successful attempts at converting an array of InAs quantum

dots or strained InGaAs, InGaAsSb, GaInAsP, GaInNAs, and GaInNAsSb quantum wells (QWs) into active regions have already been made.

A combination of the burried tunnel junction (BTJ) concept and hybrid integration of the Bragg mirrors, which feature high thermal conductivity and reflectivity, with an optical cavity based on InAlGaAsP/InP is a promising solution for long-wavelength VCSELs. InAlGaAs QWs, which have a relatively large thickness and thus provide high values of longitudinal optical confinement factor Γ_z (defined by the overlap of the fundamental mode with the active region in the longitudinal direction), are used widely as an active region. Such QWs are also more thermally stable than InGaAsP QWs, which are characterized by intense Auger recombination [5–7]. The concentration of aluminum in QWs for VCSELs operating in the 1300 nm spectral range needs to be increased considerably (up to 20%) relative to the one typical of VCSELs operating in the 1550 nm range [8]. On the one hand, this makes it possible to raise the degree of localization of carriers in an active region [9]. On the other hand, the Shockley–Read–Hall (SRH) nonradiative recombination also intensifies, thus inducing an increase in threshold currents [8,10].

The use of InGaAs QWs instead of InAlGaAs QWs potentially allows one to evade problems associated with the SRH nonradiative recombination of carriers. A reduced barrier thickness combined with an increase in the number of InGaAs QWs [11] provides an opportunity to maintain relatively high (compared to InAlGaAs QWs) values of factor Γ_z in this case [8,12]. At the same time, it should be noted that the use of ternary InGaAs solid alloys instead of quaternary InAlGaAs ones necessitates a reduction in QW thickness. The resulting characteristic thickness of strained InGaAs QWs for active regions of the 1300 nm spectral range does not exceed 1 nm. This has a negative effect on the modal gain (due to Γ_z reduction) and translates into extremely weak localization of carriers in thin QWs and, consequently, low temperature stability of VCSEL parameters.

The use of a system of tunnel-connected QWs (short-period superlattice (SL)), where the splitting of size quantization levels in tunnel-connected wells leads to the formation of energy minibands [13], is an alternative solution. It potentially allows one to improve carrier localization and obtain significantly higher values of Γ_z than those typical of thin InGaAs QWs [14]. It should be noted that one may adjust the miniband width efficiently by varying the thickness of QWs and barrier layers. The sluggishness of metalorganic chemical vapor deposition (MOCVD) makes it hard to form sharp heteroboundary profiles [15,16], while molecular beam epitaxy (MBE) offers exciting possibilities for the fabrication of active regions based on short-period SLs, since it allows for atomic-level control over the growth of epitaxial layers.

In the present study, the results of examination of the structural quality and analysis of the optical gain of short-period MBE InGaAs/InAlGaAs SLs, which are proposed to be used as active regions of VCSELs operating in the 1300 nm spectral range, are reported.

1. Experiment

Test structures on InP substrates were grown by MBE using a Riber 49 setup to examine the structural and optical characteristics of short-period InGaAs/InAlGaAs SLs. Thee structures contained an $In_{0.53}Ga_{0.27}Al_{0.2}As$ carrier collection layer with a thickness of ~ 90 nm that was bounded from the substrate and surface sides by $In_{0.52}Al_{0.48}As$ barrier layers with a thickness of 200 and 30 nm, respectively. In order to prevent surface oxidation, a cap $In_{0.53}Ga_{0.27}Al_{0.2}As$ layer with a thickness of 5 nm was also deposited. A short-period SL with 24 pairs of alternating $In_{0.6}Ga_{0.4}As$ QW layers and $In_{0.53}Ga_{0.27}Al_{0.2}As$ barrier layers with an overall thickness of ~ 70 nm was positioned in the middle of the $In_{0.53}Ga_{0.27}Al_{0.2}As$ carrier collection layer. The thicknesses of QW and barrier layers of the test structure were chosen so as to maintain intense photoluminescence around 1300 nm [17].

The X-ray diffraction curves were measured with a Bruker D8 Discover complex using the method of high-resolution X-ray diffractometry. A high-brightness tube with a rotating copper anode was used as the radiation source. The half-width of the initial beam did not exceed 12″ owing to the use of a Ge (220) quadruple slit monochromator crystal. The reciprocal space was mapped by measuring sets of X-ray diffraction curves in the vicinity of symmetric (004) and antisymmetric (224) InP reflections.

The optical properties of the test InGaAs/InAlGaAs SL structure were examined using the photoluminescence (PL) method. A solid-state Yag:Nd laser with an operating wavelength of 532 nm and an output optical power up to 350 mW was used to excite PL. The optical pump power was adjusted controllably with the use of neutral light filters, and the diameter of a focused laser spot was on the order of 65 μm. The optical system was used to focus the sample PL emission onto the entrance slits of an MDR-23 monochromator. The PL signal was detected by a single-channel cooled Ge photodiode (SRS 510, Stanford Research Systems) in the lock-in mode.

The amplification performance of the active region based on an InGaAs/InAlGaAs SL was evaluated in accordance with the procedure that involves the examination of static VCSEL characteristics as functions of the optical losses [18]. The geometry of a vertical microcavity with intracavity contacts and current confinement based on the BTJ concept was used as the baseline VCSEL design. The VCSEL heterostructure was formed by the sequential double fusion of the InAlGaAs/InP optical cavity heterostructure with the top DBR heterostructure based on 21.5 pairs of $Al_{0.91}Ga_{0.09}As$/GaAs and the bottom DBR heterostructure based on 35.5 pairs of $Al_{0.91}Ga_{0.09}As$/GaAs (this design is hereinafter referred to as WF–VCSEL). A detailed description of the heterostructure, the device design, and the

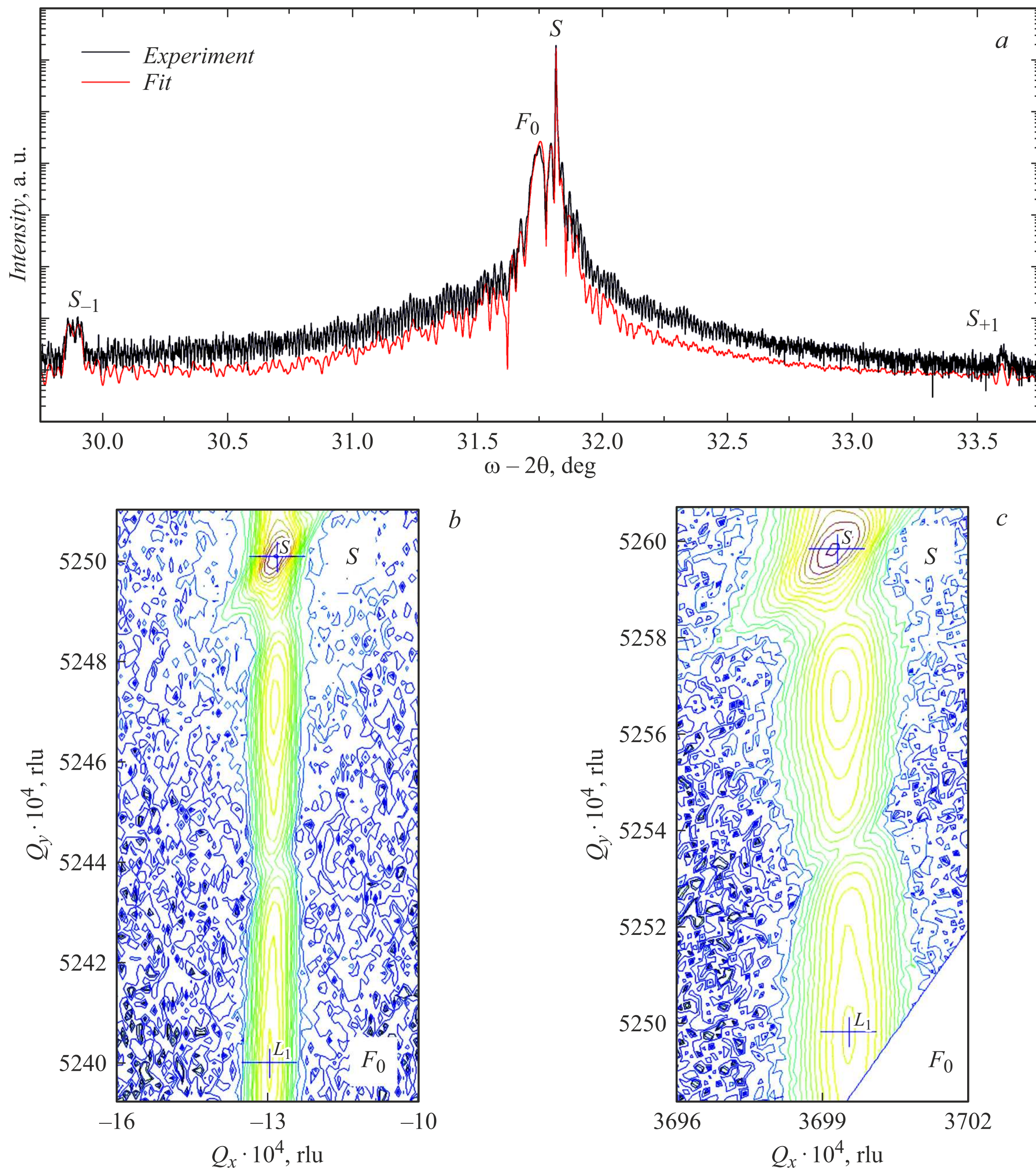

Figure 1. Results of X-ray diffraction analysis for the InGaAs/InAlGaAs SL test structure: *a* — experimental and calculated X-ray diffraction curves for the symmetric (004) reflection; *b, c* — reciprocal space maps for the symmetric (004) reflection (*b*) and the antisymmetric 224 reflection (*c*).

specifics of formation of the WF−VCSEL heterostructure by wafer fusion is given in [19,20].

2. Results and discussion

Figure 1, *a* presents the experimental and calculated X-ray diffraction curves for the symmetric (004) reflection of the InGaAs/InAlGaAs SL test structure. Zero peak F_0 of the periodic structure, which corresponds to the average SL composition, and first-order satellite peaks S_{-1}, S_{+1}, which provide information on the SL period, are visible in the rocking curve. The average composition peak (F_0) is located to the left of substrate peak S. According to the results of numerical simulation of diffraction curves within the dynamic theory of X-ray diffraction, the InGaAs/InAlGaAs SL consists of alternating layers of InGaAs QWs with a thickness of 0.6 nm and InAlGaAs barrier layers with a thickness of 2.2 nm; the average molar fraction

of indium in the SL layers was estimated at 0.55. It should be noted that the aluminum and gallium content of lattice-matched InAlGaAs layers was determined more accurately with the use of PL spectroscopy. Mismatch $\varepsilon = (\Delta a/a)_\perp = (\sin\theta_S/\sin\theta_{F_0} - 1)$ between the average lattice constant of the InGaAs/InAlGaAs SL and the lattice constant of the InP substrate in the perpendicular direction (hereinafter referred to as the lattice mismatch) is defined by the difference in angular positions of the zero peak of the periodic structure (θ_0) and substrate peak θ_S [21]. The estimate of lattice mismatch ε was $\sim +0.01\%$. This value correlates with the data for the active region of VCSELs operating in the 1300 nm spectral range based on strained ($\varepsilon = +1\%$) InAlGaAs QWs with strain compensation by InAlGaAs barrier layers ($\varepsilon = -0.9\%$) [22]. For comparison, the lattice mismatch of layers of the active region of the 1550 nm spectral range based on strained InGaAs QWs ($\varepsilon = +1.45\%$) and lattice-matched InAlGaAs barrier layers is $+0.29\%$ [23], and the mismatch for strained InAlGaAs QWs ($\varepsilon = +1.25\%$ and $+1.75\%$) and lattice-matched InAlGaAs barrier layers is as high as $+0.57\%$ and $+0.71\%$, respectively [24]. It should be noted that a short-period InGaAs/InAlGaAs SL offers more degrees of freedom in terms of strain management in SL layers than an active region based on strained In(Al)GaAs QWs. This is crucial for increasing the differential gain in the active region.

To perform a more in-depth analysis, reciprocal space maps were measured for the symmetric (004) and antisymmetric (224) reflections along the [110] direction at a substrate rotation angle φ of 0 and 90°. The key results are presented in Fig. 1, *b, c*). Characteristic peaks corresponding to substrate peak S and zero peak F_0 of the periodic structure are seen in these reciprocal space maps. The high intensity and small half-width of the zero peak of the periodic structure and the lack of severe distortions of peak shape in the reciprocal space maps are indicative of a high degree of crystalline perfection of the SL heterostructure. A small deviation in the direction of the reciprocal lattice vector (Q_x) of the position of zero peak F_0 of the periodic structure with respect to the position of substrate peak S found in measurements for the antisymmetric (224) reflection is indicative of a slight strain relaxation in the structure [25,26]. The estimated relaxation value is $\sim 11\%$.

Fig. 2 shows the PL spectra of the InGaAs/InAlGaAs SL test structure measured at 25 and 100°C. It is evident that the PL spectrum at low pump power densities has its maximum at a wavelength of ~ 1320 nm (0.93 eV), which corresponds to the transition energy of the lower SL miniband formed by the ground size quantization levels of tunnel-connected InGaAs QWs. As the optical pump power density increases from ~ 0.01 to 5 kW/cm^2 (this corresponds to an optical pump power range of $\sim 0.3-150$ mW), the PL maximum shifts gradually toward shorter wavelengths due to the filling of states

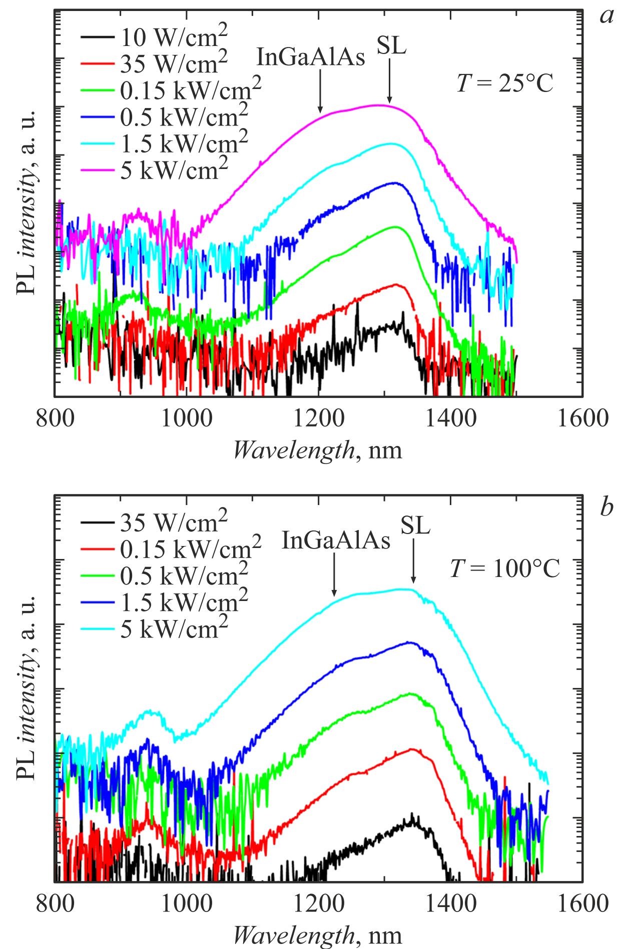

Figure 2. Photoluminescence spectra of the InGaAs/InAlGaAs SL test structure corresponding to different levels of optical pump power measured at 25 (*a*) and 100°C (*b*).

in the lower SL miniband. In addition, the PL spectrum width increases with increasing pump power density owing to the intensification of PL in the short-wavelength part of the spectrum. Apparently, this is attributable to the existence of several size quantization levels in the initial InGaAs QWs, which translates into the emergence of several SL minibands. At optical pump power densities in excess of ~ 0.5 kW/cm^2, the PL spectra contain a well-pronounced peak in the region of 1220 nm from the InAlGaAs carrier collection layer. This is indicative of the gradual saturation of emission through optical SL transitions. The shapes of spectra measured at different temperatures vary in a similar fashion; the only difference is that the PL spectrum maximum shifts toward longer wavelengths as the temperature increases.

The results of measurements of PL spectra may be used to analyze the dependence of the integrated PL intensity on the optical pump power density. The *ABC* model of recombination processes is convenient for this purpose [27]. If the system is in equilibrium, the recombination rate R

may be equated to the carrier generation rate G:

$$G \sim R = An + Bn^2 + Cn^3, \quad (1)$$

where n is the carrier density (under the assumption that the densities of electrons and holes are equal), A_n is the SRH recombination (nonradiative recombination) rate, Bn^2 is the radiative recombination rate, and Cn^3 is the Auger recombination rate. The optical pump power density P is proportional to the carrier generation rate G. At low levels of the optical pump power density, the SRH recombination mechanism is dominant, while Auger recombination prevails at high pump power densities, since higher-order terms start producing a more significant contribution to the recombination process as the optical pump power density increases. At moderate optical pump power densities, the Bn^2 radiative recombination mechanism should be dominant.

The relative contributions of different recombination processes to emission may be estimated by analyzing the dependence of the integrated PL intensity on the optical pump power density and approximating this dependence with power function P^k. Fig. 3 shows the experimental dependences of the integrated PL intensity (I_{PL}) on the optical pump power density (P) measured at 25 and 100°C and plotted in log-log scale. It can be seen that power exponent k is close to unity at a temperature of 25°C and a low optical pump density. At higher pump power levels, k increases to ~ 1.8, which is likely to be attributable to the increasing contribution of emission from the InAlGaAs carrier collection layer, where the nonradiative recombination process is more pronounced [8,10], to the overall PL intensity. As the temperature grows, the initial section with the PL intensity proportional to the optical pump power density $(k \sim 1)$ vanishes; at 100°C, power exponent k becomes close to ~ 1.7. The obtained experimental data suggest that the contribution of Auger recombination is insignificant even at elevated temperatures and remains imperceptible within the entire studied range of optical pump power densities.

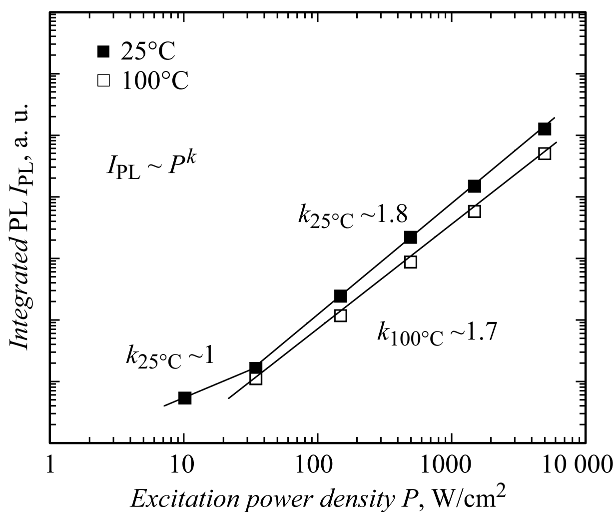

Figure 3. Dependence of the integrated photoluminescence intensity on the optical pump power density and approximating P^k curves at different temperatures.

The proposed InGaAs/InAlGaAs SL was proven to be a fine active region of VCSELs operating in the 1300 nm spectral range that were fabricated by wafer fusion (WF–VCSEL), with carrier injection via n-type intracavity contacts and a composite n^+-InGaAs/p^+–InGaAs/p^+–InAlGaAs TJ [20]. To strike a compromise between relatively low threshold currents and high differential gain at moderate temperatures (20–60°C), the SL layer thicknesses were adjusted so that the projective resonance wavelength of the microcavity got shifted by ~ 20 nm toward longer wavelengths relative to the peak of the PL spectrum of the active region, which is correlated tentatively with the maximum of the gain spectrum. It should be noted that the reduction in QW thickness and the increase in barrier layer thickness lead to a short-wave shift of the PL peak corresponding to the lower miniband [17]. However, the power exponent of function P_k is not affected visibly by variations of the thickness ratio of QWs and the SL barrier layer if the primary PL peak remains within the wavelength range of 1260–1320 nm.

As is known, the condition for the initiation and stabilization of steady-state lasing consists in achieving a balance between modal gain G_{th} and the sum of optical losses [4]:

$$G_{th} = \Gamma_z \Gamma_{tr} g_{th} = \alpha_{\text{int}} + \alpha_m, \quad (2)$$

where g_{th} is the material gain of the active region at the lasing threshold, α_m are mirror losses, α_{int} are internal optical losses, and Γ_z and Γ_{tr} are the longitudinal and transverse optical confinement factors, respectively.

In the case of VCSELs, factor Γ_z is commonly calculated within the 1D model of a vertical microcavity using the transfer matrix method [28], while factor Γ_{tr} may be estimated using the two-dimensional effective waveguide model [29]. The value of Γ_z of the WF–VCSEL with an SL active region is more than 1.5 times higher (as high as $\sim 4.7\%$) than the corresponding parameter of VCSELs with an active region based on InAlGaAs QWs [30]. When the BTJ concept is implemented, the degree of transverse optical confinement depends on the lateral size of the BTJ mesa, the TJ etching depth, and the modification of surface relief, which was formed in TJ layers, in the process of subsequent regrowth with the intracavity contact layer. The needed calculations were carried out within the simplified two-dimensional model of a five-step effective waveguide [31]. The value of Γ_{tr} for the fundamental mode of the studied WF–VCSEL structure is close to 100% for wide-aperture devices (with an BTJ mesa diameter $\geq 6\,\mu$m).

Several major mechanisms of internal optical losses may be identified for VCSELs: optical absorption, lateral leakage of optical modes (so-called waveguide modes), and lateral losses due to light scattering on local refraction index inhomogeneities in the lateral direction and (or) diffraction at the optical aperture that provides transverse optical

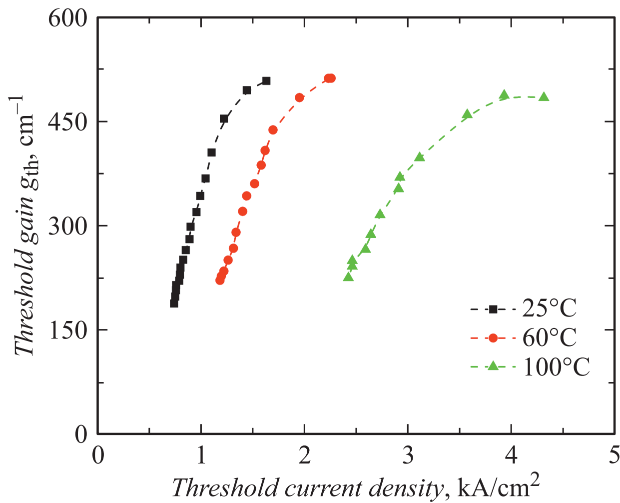

Figure 4. Dependences of the material gain at the lasing threshold on the threshold current density at different temperatures for the WF–VCSEL with an active region based on an InGaAs/InAlGaAs SL and an BTJ mesa diameter of 6 μm.

confinement [4]. Taking the results of numerical modeling of lateral losses in WF–VCSELs [32] and the nature of variation of watt–ampere characteristics of the fabricated WF–VCSELs with temperature into account, one may assume that the internal optical losses should be minimized in wide-aperture lasers (with an BTJ mesa diameter $\geq 6\,\mu$m) with the optical absorption at free carriers and the interband absorption producing the primary contribution to internal losses α_{int}. The level of internal optical losses may be estimated by analyzing the dependence of external quantum efficiency η on the mirror losses with the use of methods for the variation of the reflection coefficient of the output DBR at the resonance microcavity wavelength [18,33] in accordance with the following expressions:

$$\eta^{-1} = \eta_{\text{int}}^{-1}(1 + \alpha_{\text{int}}/\alpha_m), \tag{3}$$

$$\alpha_m = -\ln\sqrt{R_T R_B}/L_{\text{eff}}, \tag{4}$$

where η_{int} is the efficiency of current injection of carriers, L_{eff} is the effective cavity length with account for penetration of the electromagnetic field into mirrors ($\sim 2.4\,\mu$m), and R_B and R_T are the reflection coefficients of the near 100% mirror (bottom DBR) and the output mirror (top DBR) at the resonance VCSEL microcavity wavelength, respectively. The dependences of refraction indices of DBR materials on the wavelength and temperature [34,35] were taken into account in calculations of the reflection coefficients of mirrors by the transfer matrix method.

Fig. 4 shows the dependences of material gain g_{th} at the lasing threshold on threshold current density J_{th} obtained at different temperatures under varying mirror losses for the WF–VCSEL with an BTJ diameter of 6 μm. The diffusion length of carriers in the active region ($\sim 2.2\,\mu$m), which was determined by analyzing the dependence of the threshold current on the BTJ size, was taken into account in calculations of the current density. The obtained $g_{th}(J_{th})$ dependences are approximated closely in a wide range of current densities by a logarithmic function that factors in the gain saturation at high carrier densities:

$$g = g_0 \ln(\eta_{\text{int}} J/J_{tr}), \tag{5}$$

where g_0 is the gain parameter and J_{tr} is the transparent current density. It should be noted that this empirical relation characterizes well the optical gain of bulk materials and QWs [36], but does not take into account the specific features of shape of the gain spectrum of the active region and its variation with current and temperature. Specifically, this leads to a significant deviation of the $g_{th}(J_{th})$ dependence from the logarithmic function at high current densities, which correspond to a high level of mirror losses α_m, due to the variation of the actual value of spectral mismatch between the resonance wavelength and the gain spectrum (induced by self-heating effects).

Exponential functions with a characteristic temperature are used often to characterize the temperature behavior of the gain parameter and the transparent current density of edge-emitting lasers similar to the temperature behavior of the differential efficiency (exponential reduction) and the threshold current density (exponential growth) [37,38]. Temperature dependence $J_{tr}(T)$ of the transparent current density is defined by the relation between nonradiative, radiative, and Auger recombination processes for each specific laser type and material system of the active region. For example, lasers with InGaAsP–InP QWs dominated by Auger recombination feature a low temperature dependence of the transparent current with characteristic temperature $T_{tr} \sim$ 50–80 K [37], while the transparent current in lasers with InGaAs–GaAs QWs dominated by nonradiative recombination is almost independent of temperature (characteristic temperature $T_{tr} > 300$ K) [38]. Although the maximum material gain decreases at higher temperatures due to the broadening of the Fermi–Dirac distribution function [6], gain parameter g_0 for lasers based on InGaAsP–InP QWs [37], highly strained InGaAs–GaAs QWs [37], and InGaAsN–GaAs QWs [39] has a low temperature sensitivity (the corresponding characteristic temperature is $T_g > 250$ K). Thus, in view of the PL spectroscopy results, the gain parameter and the transparent current density for the InGaAs/InAlGaAs SL is expected to be only weakly sensitive to temperature variations.

Fig. 5 presents the values of g_0 and J_{tr} at different temperatures calculated based on the experimental $g_{th}(J_{th})$ dependences for the WF–VCSEL with an BTJ diameter of 6 μm. While the threshold gain in the analysis of edge-emitting lasers corresponds to the maximum of the gain spectrum, a similar analysis for VCSELs is practically performed at the resonance wavelength of the microcavity. Therefore, one needs to take into account the effect of spectral mismatch between the resonance wavelength and the gain spectrum peak in the analysis of temperature

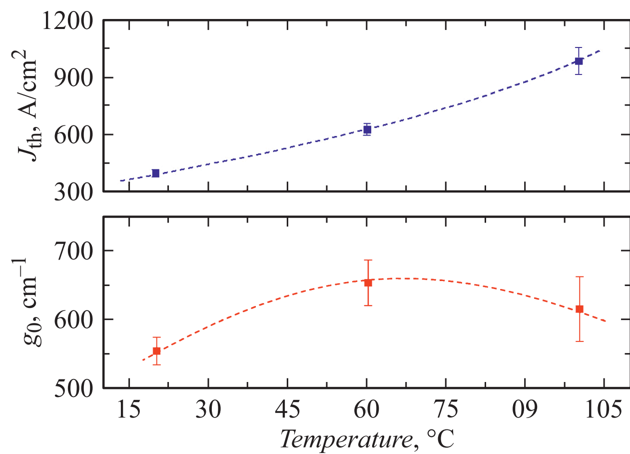

Figure 5. Temperature dependences of the gain parameter and the transparent current density calculated based on the experimental data from Fig. 4 for the WF–VCSEL with an active region based on the InGaAs/InAlGaAs SL and an BTJ mesa diameter of 6 μm.

dependences of g_0 and J_{tr} values measured for VCSELs. Owing to this effect, the temperature dependences of the threshold gain and the threshold current of VCSELs are more complex than those of edge-emitting lasers [40,41]. According to Fig. 5, the transparent current density and the gain parameter first increase with temperature, but start decreasing at temperatures above 60°C. Since the PL spectra are in a first approximation correlated with the gain spectrum, we assume that the studied devices have zero spectral mismatch (i.e., the gain peak coincides with the resonance wavelength of the VCSEL microcavity) at a temperature of 50–60°C. This is the temperature range where one may obtain reliable data on the maximum optical gain and the transparent current of the active region based on the InGaAs/InAlGaAs SL. The following values were determined for the transparent current density and the gain parameter: ~ 630 A/cm^2 and ~ 650 cm^{-1}.

It appears to be not quite correct to compare the obtained data directly with the published reports on edge-emitting lasers, since the vertical microcavity of a VCSEL is designed so that optical emission generated in the active region propagates perpendicularly to its plane, thus imposing a strong restriction on the modal gain. At the same time, although 1300 nm range VCSELs based on three InGaAsN–GaAs QWs [42], InGaAsNSb–GaAs QWs [3], or six InAlGaAs–InP QWs [8,30] have been fabricated and tested successfully, the material gain and the transparent current density for the indicated active regions have not been reported. Therefore, a direct comparison is impossible. It should be noted that the restriction on the number of QWs in these types of active regions stems from the technological specifics of the epitaxial synthesis of strained QWs. Potentially feasible versions of QW-based active regions may be examined to perform a plausible comparison of an active region based on a short-period InGaAs/InAlGaAs SL with alternative designs. The obtained g_0 values correlate well not only with the data obtained at 20–25°C for InAsP–InP QWs emitting in the 1300 nm spectral range ($g_0 \sim$ 650–720 cm^{-1}) [43], InGaAsP–InP QWs emitting at 1550 nm ($g_0 \sim 466$ cm^{-1}) [36], InGaAs–InP QWs emitting at 1550 nm ($g_0 \sim$ 516–630 cm^{-1}) [36,44], and InAlGaAs–InP QWs emitting at 1300 nm (~ 884 cm^{-1}), but also with the parameters of InGaAsN–GaAs QWs emitting in the 1300 nm spectral range in the considered range of temperatures 50–60°C ($g_0 \sim 750$ cm^{-1}) [39]. In addition, the attained value is consistent with the data referred to the actual number of wells for highly strained InGaAsN–GaAs QWs emitting in the 1300 nm spectral range ($\sim$ 84–240 A/cm^2 per 1 QW at 20°C) [39,45,46] and strained InAlGaAs–InP QW emitting at 1300 nm ($\sim$ 177–250 A/cm^2 per 1 QW at 20–60°C) [47].

Conclusion

Original heterostructures for active regions based on short-period InGaAs/InAlGaAs superlattices emitting in the 1300 nm spectral range were proposed and fabricated. The use of molecular beam epitaxy ensured high structural quality of heterostructures, which was verified by high-resolution X-ray diffractometry. The analysis of reciprocal space maps did not reveal any significant shape distortions of the average SL composition peak, but provided the evidence of strain relaxation ($\sim 11\%$) in the structure. According to the results of numerical analysis, the average molar fraction of indium in the short-period SL based on alternating $In_{0.6}Ga_{0.4}As$ QW layers and $In_{0.53}Ga_{0.27}Al_{0.2}As$ barrier layers with an overall thickness of ~ 70 nm is 0.55. This corresponds to a mismatch of $\sim +0.01\%$ between the lattice constants of the SL and the substrate.

According to the results of photoluminescence spectroscopy, heterostructures based on the InGaAs/InAlGaAs SL have the capacity for efficient luminescence in the 1260–1320 nm wavelength range. Adjusting the QW and barrier layer thicknesses, one may control the position of the PL peak corresponding to optical transitions in the lower SL miniband. It follows from the results of analysis of the integrated PL intensity at different levels of pumping of the SL-based active region heterostructure within the *ABC* model of recombination processes that the contribution of Auger recombination is insignificant in the studied pump power range.

The optical gain and the transparent current density at various values of the spectral mismatch between the resonance wavelength and the gain spectrum peak were estimated by examining the influence of outcoupling losses and temperature on the parameters of a VCSEL with an active region based on the InGaAs/InAlGaAs SL. The gain parameter was estimated at ~ 650 cm^{-1} using the common logarithmic approximation of the dependence of gain on the pump current density at zero spectral mismatch. Since the corresponding longitudinal optical confinement factor

is 1.5 times higher than the one for an active region based on InAlGaAs QWs, the resulting modal gain is fairly high. A transparent current density of $\sim 630\,\mathrm{A/cm^2}$ at 60°C was achieved. This value is comparable with the results for strained InAlGaAs−InP QWs and highly strained InGaAsN−GaAs QWs emitting in the 1300 nm spectral range. Moderate values of the transparent current density coupled with a greater (compared to active regions based on strained InAlGaAs QWs) flexibility of strain management in short-periodic SL layers offer ample opportunities for enhancing the differential gain of active regions emitting in the 1300 nm spectral range.

Acknowledgments

A.M. Nadtochii acknowledges support from the Fundamental Research Program of the National Research University Higher School of Economics in optical measurements.

Funding

This study was supported financially by the Ministry of Science and Higher Education of the Russian Federation, research project No. 2019-1442. X-ray diffraction curves were analyzed using the equipment provided by the Materials Science and Diagnostics in Advanced Technologies common use center (Ioffe Institute, St. Petersburg).

Conflict of interest

The authors declare that they have no conflict of interest.

References

[1] M.V.R. Murty, J. Wang, A.L. Harren, A.-N. Cheng, D.W. Dolfi, Z.-W. Feng, A. Sridhara, S.T. Joyo, J. Chu, L.M. Giovane. IEEE Photonics Technol. Lett., **33** (16), 812 (2021). DOI: 10.1109/lpt.2021.3069146

[2] Z. Ruan, Y. Zhu, P. Chen, Y. Shi, S. He, X. Cai, L. Liu. J. Lightwave Technol., **38** (18), 5100 2020. DOI:10.1109/jlt.2020.2999526

[3] M. Gębski, D. Dontsova, N. Haghighi, K. Nunna, R. Yanka, A. Johnson, R. Pelzel, J.A. Lott. OSA Continuum, **3** (7), 1952 (2020). DOI: 10.1364/osac.396242

[4] *VCSELs: Fundamentals, Technology and Applications of Vertical-Cavity Surface-Emitting Lasers*. Springer Series in Optical Sciences, ed. R. Michalzik (Springer, Berlin, Heidelberg, 2013) DOI: 10.1007/978-3-642-24986-0

[5] J. Minch, S.H. Park, T. Keating, S.L. Chuang. IEEE J. Quant. Electron., **35** (5), 771 (1999). DOI: 10.1109/3.760325

[6] J.C.L. Yong, J.M. Rorison, I.H. White. IEEE J. Quant. Electron., **38** (12), 1553 (2002). DOI: 10.1109/jqe.2002.805100

[7] Y.-K. Kuo, S.-H. Yen, M.-W. Yao, M.-L. Chen, B.-T. Liou. Opt. Commun., **275** (1), 156 (2007). DOI: 10.1016/j.optcom.2007.02.025

[8] M. Muller, C. Grasse, M.C. Amann. In *Proc. 2012 14th International Conference on Transparent Optical Networks (ICTON)* (IEEE, Coventry, UK, 2012) DOI: 10.1109/icton.2012.6254394

[9] S. Spiga, M.C. Amann. „High-Speed InP-Based Long-Wavelength VCSELs,“ *Green Photonics and Electronics*, ed. G. Eisenstein, D. Bimberg. (Springer, Cham, 2017), p. 17−35. DOI: 10.1007/978-3-319-67002-7_2

[10] C. Grasse, M. Mueller, T. Gruendl, G. Boehm, E. Roenneberg, P. Wiecha, J. Rosskopf, M. Ortsiefer, R. Meyer, M.-C. Amann. J. Cryst. Growth, **370**, 217 (2013). DOI: 10.1016/j.jcrysgro.2012.06.051

[11] E.S. Kolodeznyi, S.S. Rochas, A.S. Kurochkin, A.V. Babichev, I.I. Novikov, A.G. Gladyshev, L.Y. Karachinskii, D.V. Denisov, Y.K. Bobretsova, A.A. Klimov, S.A. Blokhin, K.O. Voropaev, A.S. Ionov. Opt. Spectr., **125** (2), 238 (2018). DOI: 10.1134/s0030400x18080143

[15] M. Muller, P. Debernardi, C. Grasse, T. Grundl, M.-C. Amann. IEEE Photonics Technol. Lett., **25** (2), 140 (2013). DOI: 10.1109/lpt.2012.2229975

[13] J. Faist, F. Capasso, D.L. Sivco, C. Sirtori, A.L. Hutchinson, A.Y. Cho. Science, **264** (5158), 553 (1994). DOI: 10.1126/science.264.5158.553

[14] L.Y. Karachinsky, I.I. Novikov, A.V. Babichev, A.G. Gladyshev, E.S. Kolodeznyi, S.S. Rochas, A.S. Kurochkin, Y.K. Bobretsova, A.A. Klimov, D.V. Denisov, K.O. Voropaev, A.S. Ionov, V.E. Bougrov, A.Y. Egorov. Opt. Spectr., **127** (6), 1053 (2019). DOI: 10.1134/s0030400x19120099

[15] C.A. Wang, B. Schwarz, D.F. Siriani, L.J. Missaggia, M.K. Connors, T.S. Mansuripur, D.R. Calawa, D. McNulty, M. Nickerson, J.P. Donnelly, K. Creedon, F. Capasso. IEEE J. Sel. Top. Quant. Electron., **23** (6), 1 (2017). DOI: 10.1109/jstqe.2017.2677899

[16] B. Schwarz, C.A. Wang, L. Missaggia, T.S. Mansuripur, P. Chevalier, M.K. Connors, D. McNulty, J. Cederberg, G. Strasser, F. Capasso. ACS Photonics, **4** (5), 1225 (2017). DOI: 10.1021/acsphotonics.7b00133

[17] S.S. Rochas, I.I. Novikov, A.G. Gladyshev, E.S. Kolodeznyi, A.V. Babichev, V.V. Andryushkin, V.N. Nevedomskii, D.V. Denisov, L.Ya. Karachinsky, A.Yu. Egorov, V.E. Bougrov. Tech. Phys. Lett., 46 (11), 1128 (2020). DOI: 10.1134/S1063785020110267

[18] G.M. Yang, M.H. MacDugal, V. Pudikov, P.D. Dapkus. IEEE Photon. Technol. Lett., **7** (11), 1228 (1995). DOI: 10.1109/68.473454

[19] S.A. Blokhin, S.N. Nevedomsky, M.A. Bobrov, N.A. Maleev, A.A. Blokhin, A.G. Kuzmenkov, A.P. Vasyl'ev, S.S. Rohas, A.V. Babichev, A.G. Gladyshev, I.I. Novikov, L.Ya. Karachinsky, D.V. Denisov, K.O. Voropaev, A.S. Ionov, A.Yu. Egorov, V.M. Ustinov. Semiconductors, **54**, 1276 (2020). DOI: 10.1134/S1063782620100048

[20] S. Blokhin, A. Babichev, A. Gladyshev, L. Karachinsky, I.Novikov, A. Blokhin, S. Rochas, D. Denisov, K. Voropaev, A. Ionov, N. Ledentsov, A. Egorov. Electron. Lett., (just accepted) (2021). DOI: 10.1049/ell2.12232

[21] D. Pierścińska, P. Gutowski, G. Hałdaś, A. Kolek, I. Sankowska, J. Grzonka, J. Mizera, K. Pier siński, M. Bugajski. Semicond. Sci. Technol., **33** (3), 035006 (2018). DOI: 10.1088/1361-6641/aaa91a

[22] N. Volet, Optical Mode Control in Long-Wavelength Vertical-Cavity Surface-Emitting Lasers. (Diss. Ph. D. thesis, 2014), DOI: 10.5075/epfl-thesis-6064

[23] A.V. Babichev, L.Y. Karachinsky, I.I. Novikov, A.G. Gladyshev, S.A. Blokhin, S. Mikhailov, V. Iakovlev, A. Sirbu, G. Stepniak, L. Chorchos, J.P. Turkiewicz, K.O. Voropaev, A.S. Ionov, M. Agustin, N.N. Ledentsov, A.Y. Egorov. IEEE J. Quant. Electron., **53** (6), 1 (2017). DOI: 10.1109/jqe.2017.2752700

[24] S. Spiga, D. Schoke, A. Andrejew, G. Boehm, M.-C. Amann. J. Lightwave Technol., **35** (15), 3130 (2017). DOI: 10.1109/jlt.2017.2660444

[25] I. Sankowska, P. Gutowski, A. Jasik, K. Czuba, J. Dabrowski, M. Bugajski. J. Appl. Crystallogr., **50** (5), 1376 (2017). DOI: 10.1107/s1600576717011815

[26] G. Capuzzo, D. Kysylychyn, R. Adhikari, T. Li, B. Faina, A. Tarazaga Martín-Luengo, A. Bonanni. Sci. Rep., **7** (1), 42697 (2017). DOI: 10.1038/srep42697

[27] I.B. Karomi, A.T. Zakar, M.S. Al-Ghamdi. IOP Conf. Ser.: Mater. Sci. Eng., **1126** (1), 012004 (2021). DOI: 10.1088/1757-899x/1126/1/012004

[28] Y. Huang, Z. Pan, R. Wu. J. Appl. Phys., **79** (8), 3827 (1996). DOI: 10.1063/1.361809

[29] G.R. Hadley. Opt. Lett., **20** (13), 1483 (1995). DOI: 10.1364/OL.20.001483

[30] D. Ellafi, V. Iakovlev, A. Sirbu, G. Suruceanu, Z. Mickovic, A. Caliman, A. Mereuta, E. Kapon. IEEE J. Sel. Top. Quant. Electron., **21** (6), 414 (2015). DOI: 10.1109/jstqe.2015.2412495

[31] S.A. Blokhin, M.A. Bobrov, A.A. Blokhin, A.P. Vasil'ev, A.G. Kuz'menkov, N.A. Maleev, S.S. Rochas, A.G. Gladyshev, A.V. Babichev, I.I. Novikov, L.Ya. Karachinsky, D.V. Denisov, K.O. Voropaev, A.S. Ionov, A.Yu. Egorov, V.M. Ustinov. Tech. Phys. Lett. **46**, 1257 (2020). DOI: 10.1134/S1063785020120172

[32] J. Bengtsson, J. Gustavsson, Å˙ Haglund, A. Larsson, A. Bachmann, K. Kashani-Shirazi, M.-C. Amann. Opt. Express, **16** (25), 20789 (2008).

[33] S.A. Blokhin, M.A. Bobrov, A.A. Blokhin, A.G. Kuzmenkov, N.A. Maleev, V.M. Ustinov, E.S. Kolodeznyi, S.S. Rochas, A.V. Babichev, I.I. Novikov, A.G. Gladyshev, L.Ya. Karachinsky, D.V. Denisov, K.O. Voropaev, A.S. Ionov, A.Yu. Egorov. Opt. Spectr. **127** (1), 140 (2019). DOI: 10.1134/S0030400X1907004X

[34] S. Adachi. J. Appl. Phys. **66** (12), 6030 (1989). DOI: 10.1063/1.343580

[35] S. Gehrsitz, F.K. Reinhart, C. Gourgon, N. Herres, A. Vonlanthen, H. Sigg. J. Appl. Phys., **87** (11), 7825 (2000). DOI: 10.1063/1.373462

[36] T.A. DeTemple, C.M. Herzinger. IEEE J. Quant. Electron., **29** (5), 1246 (1993). DOI: 10.1109/3.236138

[37] T. Higashi, T. Yamamoto, S. Ogita, M. Kobayashi. IEEE J. Sel. Topics Quant. Electron., **3** (2), 513 (1997). DOI: 10.1109/islc.1996.553742

[38] N. Tansu, Y.-L. Chang, T. Takeuchi, D.P. Bour, S.W. Corzine, M.R.T. Tan, L.J. Mawst. IEEE J. Quant. Electron., **38** (6), 640 (2002). DOI: 10.1109/jqe.2002.1005415

[39] T. Kageyama, T. Miyamoto, S. Makino, Y. Ikenaga, F. Koyama, K. Iga. IEICE Trans. Electron., $\mathbf{E85-C(1)}$, 71 (2002). DOI: 10.7567/ssdm.1999.le-1-1

[40] J. Piprek, Y.A. Akulova, D.I. Babic, L.A. Coldren, J.E. Bowers. Appl. Phys. Lett., **72** (15), 1814 (1998). DOI: 10.1063/1.121318

[41] S. Mogg, N. Chitica, U. Christiansson, R. Schatz, P. Sundgren, C. Asplund, M. Hammar. IEEE J. Quant. Electron., **40** (5), 453 (2004). DOI: 10.1109/jqe.2004.826421

[42] H. Riechert, A. Ramakrishnan, G. Steine. Semicond. Sci. Technol., **17** (8), 892–897 (2002). DOI: 10.1088/0268-1242/17/8/318

[43] H. Shimizu, K. Kumada, N. Yamanaka, N. Iwai, T. Mukaihara, A. Kasukawa. IEEE J. Quant. Electron., **36** (6), 728 (2000). DOI: 10.1109/3.845730

[44] M. Rosenzweig, M. Mohrle, H. Duser, H. Venghaus. IEEE J. Quant. Electron., **27** (6), 1804 (1991). DOI: 10.1109/3.90008

[45] N. Tansu, J.-Y. Yeh, L.J. Mawst. IEEE J. Sel. Topics Quant. Electron., **9** (5), 1220 (2003). DOI: 10.1109/jstqe.2003.820911

[46] C.Y. Liu, S.F. Yoon, W.J. Fan, J.W.R. Teo, S. Yuan. Opt. Express, **13** (22), 9045 (2005). DOI: 10.1364/opex.13.009045

[47] H. Wada, K. Takemasa, T. Munakata, M. Kobayashi, T. Kamijoh. IEEE J. Sel. Topics Quantum Electron., **5** (3), 420–427 (1999). DOI: 10.1109/2944.788400